



Deposited via The University of Sheffield.

White Rose Research Online URL for this paper:

<https://eprints.whiterose.ac.uk/id/eprint/235915/>

Version: Published Version

Article:

Abe, A., Abe, S., Akutsu, R. et al. (2025) Testing T2K's Bayesian constraints with priors in alternate parameterisations. *The European Physical Journal C*, 85 (12). 1414. ISSN: 1434-6044

<https://doi.org/10.1140/epjc/s10052-025-14836-0>

Reuse

This article is distributed under the terms of the Creative Commons Attribution (CC BY) licence. This licence allows you to distribute, remix, tweak, and build upon the work, even commercially, as long as you credit the authors for the original work. More information and the full terms of the licence here:

<https://creativecommons.org/licenses/>

Takedown







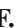













If you consider content in White Rose Research Online to be in breach of UK law, please notify us by emailing eprints@whiterose.ac.uk including the URL of the record and the reason for the withdrawal request.



Testing T2K's Bayesian constraints with priors in alternate parameterisations

T2K Collaboration

A. Abe⁶⁰, S. Abe⁶⁰, R. Akutsu¹⁵, H. Alaraki-Charles³⁴, Y. I. Alj Hakim⁵⁵, S. Alonso Monsalve¹⁰, L. Anthony²¹, S. Aoki³², K. A. Apte²¹, T. Arai⁵⁹, T. Arihara⁶³, S. Arimoto³³, Y. Ashida⁶⁹, E. T. Atkin²¹, N. Babu³⁸, V. Baranov³⁹, G. J. Barker⁷⁰, G. Barr⁴⁶, D. Barrow⁴⁶, P. Bates⁵⁷, L. Bathe-Peters⁴⁶, M. Batkiewicz-Kwasniak¹⁴, N. Baudis⁴⁶, V. Berardi²², L. Berns⁶⁹, S. Bhattacharjee³⁸, A. Blanchet¹¹, A. Blondel^{12,57}, P. M. M. Boistier⁵, S. Bolognesi⁵, S. Bordini¹², S. B. Boyd⁷⁰, C. Bronner⁷³, A. Bubak⁵⁶, M. Buizza Avanzini³⁶, J. A. Caballero⁵⁶, F. Cadoux¹², N. F. Calabria²², S. Cao²⁰, S. Cap¹², D. Carabadjac^{36,a}, S. L. Cartwright⁵⁵, M. P. Casado^{17,j}, M. G. Catanesi²², J. Chakrani³⁵, A. Chalumeau⁵⁷, D. Cherdack¹⁶, P. S. Chong⁴⁷, A. Chvirova²⁶, J. Coleman³⁷, G. Collazuol²⁴, F. Cormier⁶⁶, A. A. L. Craplet²¹, A. Cudd⁶, D. D'ago²⁴, C. Dalmazzone⁵⁷, T. Daret⁵, P. Dasgupta⁹, C. Davis⁴⁷, Yu. I. Davydov³⁹, P. de Perio²⁹, G. De Rosa²³, T. Dealtry³⁴, C. Densham⁵⁸, A. Dergacheva²⁶, R. Dharmapal Banerjee⁷², F. Di Lodovico³¹, G. Diaz Lopez⁵⁷, S. Dolan¹¹, D. Douqa¹², T. A. Doyle⁴³, O. Drapier³⁶, K. E. Duffy⁴⁶, J. Dumarchez⁵⁷, P. Dunne²¹, K. Dygnarowicz⁶⁸, A. Eguchi⁵⁹, J. Elias⁵¹, S. Emery-Schrenk⁵, G. Erofeev²⁶, A. Ershova³⁶, G. Eurin⁵, D. Fedorova²⁶, S. Fedotov²⁶, M. Feltre²⁴, L. Feng³³, D. Ferlewicz⁵⁹, A. J. Finch³⁴, M. D. Fitton⁵⁸, C. Forza²⁴, M. Friend^{15,b}, Y. Fujii^{15,b}, Y. Fukuda⁴¹, Y. Furui⁶³, J. García-Marcos⁷⁵, A. C. Germer⁴⁷, L. Giannessi¹², C. Giganti⁵⁷, M. Girgus⁶⁷, V. Glagolev³⁹, M. Gonin²⁸, R. González Jiménez⁵⁴, J. González Rosa⁵⁴, E. A. G. Goodman¹³, K. Gorshanov²⁶, P. Govindaraj⁶⁷, M. Grassi²⁴, M. Guigue⁵⁷, F. Y. Guo⁴³, D. R. Hadley⁷⁰, S. Han^{33,61}, D. A. Harris⁷⁴, R. J. Harris^{34,58}, T. Hasegawa^{15,b}, C. M. Hasnip¹¹, S. Hassani⁵, N. C. Hastings¹⁵, Y. Hayato^{29,60}, I. Heitkamp⁶⁹, D. Henaff⁵, Y. Hino¹⁵, J. Holeczek⁵⁶, A. Holin⁵⁸, T. Holvey⁴⁶, N. T. Hong Van²⁷, T. Honjo⁴⁵, M. C. F. Hooft⁷⁵, K. Hosokawa⁶⁰, J. Hu³³, A. K. Ichikawa⁶⁹, K. Ieki⁶⁰, M. Ikeda⁶⁰, T. Ishida^{15,b}, M. Ishitsuka⁶⁴, H. Ito³², S. Ito⁷³, A. Izmaylov²⁶, N. Jachowicz⁷⁵, S. J. Jenkins³⁷, C. Jesús-Valls¹¹, M. Jia⁴³, J. J. Jiang⁴³, J. Y. Ji⁴³, T. P. Jones³⁴, P. Jonsson²¹, S. Joshi⁵, M. Kabirnezhad²¹, A. C. Kaboth⁵², H. Kakuno⁶³, J. Kameda⁶⁰, S. Karpova¹², V. S. Kasturi¹², Y. Kataoka⁶⁰, T. Katori³¹, A. Kawabata³⁰, Y. Kawamura⁴⁵, M. Kawaue³³, E. Kearns^{3,c}, M. Khabibullin²⁶, A. Khotjantsev²⁶, T. Kikawa³³, S. King³¹, V. Kiseeva³⁹, J. Kisiel⁵⁶, A. Klustová²¹, L. Kneale⁵⁵, H. Kobayashi⁵⁹, L. Koch¹⁸, S. Kodama⁵⁹, M. Kolupanova²⁶, A. Konaka⁶⁶, L. L. Kormos³⁴, Y. Koshio^{44,c}, K. Kowalik⁴², Y. Kudenko^{26,d}, Y. Kudo⁷³, A. Kumar Jha⁷⁵, R. Kurjata⁶⁸, V. Kurochka²⁶, T. Kutter³⁸, L. Labarga¹, M. Lachat⁵¹, K. Lachner¹⁰, J. Lagoda⁴², S. M. Lakshmi⁵⁶, M. Lamers James⁷⁰, A. Langella²³, D. H. Langridge⁵², J.-F. Laporte⁵, D. Last⁵¹, N. Latham³¹, M. Laveder²⁴, L. Lavitola²³, M. Law³⁴, D. Leon Silverio⁷⁶, S. Levorato⁵, S. V. Lewis³¹, B. Li¹⁰, C. Lin²¹, R. P. Litchfield¹³, S. L. Liu⁴³, W. Li⁴⁶, A. Longhin²⁴, A. Lopez Moreno^{31,a}, L. Ludovici²⁵, X. Lu⁷⁰, T. Lux¹⁷, L. N. Machado¹³, L. Magaletti²², K. Mahn⁴⁰, K. K. Mahtani⁴³, M. Mandal⁴², S. Manly⁵¹, A. D. Marino⁶, D. G. R. Martin²¹, D. A. Martinez Caicedo⁷⁶, L. Martinez¹⁷, M. Martini^{57,e}, T. Matsubara¹⁵, R. Matsumoto⁶², V. Matveev²⁶, C. Mauger⁴⁷, K. Mavrokoridis³⁷, N. McCauley³⁷, K. S. McFarland⁵¹, C. McGrew⁴³, J. McKean²¹, A. Mefodiev²⁶, G. D. Megias⁵⁴, L. Mellet⁴⁰, C. Metelko³⁷, M. Mezzetto²⁴, S. Miki⁶⁰, V. Mikola¹³, E. W. Miller¹⁷, A. Minamino⁷³, O. Mineev²⁶, S. Mine^{60,4}, J. Mirabito³, M. Miura^{60,c}, S. Moriyama^{60,c}, S. Moriyama⁷³, P. Morrison¹³, Th. A. Mueller³⁶, D. Munford¹⁶, A. Muñoz^{28,36}, L. Munteanu¹¹, Y. Nagai⁹, T. Nakadaira^{15,b}, K. Nakagiri⁵⁹, M. Nakahata^{29,60}, Y. Nakajima⁵⁹, K. D. Nakamura⁶⁹, A. Nakano⁶⁹, Y. Nakano⁷⁷, S. Nakayama^{29,60}, T. Nakaya^{29,33}, K. Nakayoshi^{15,b}, C. E. R. Naseby²¹, D. T. Nguyen⁷⁸, V. Q. Nguyen³⁶, K. Niewczas⁷⁵, S. Nishimori¹⁵, Y. Nishimura³⁰, Y. Noguchi⁶⁰, T. Nosek⁴², F. Nova⁵⁸, P. Novella¹⁹, J. C. Nugent²¹, H. M. O'Keefe³⁴, L. O'Sullivan⁸, R. Okazaki³⁰, W. Okinaga⁵⁹, K. Okumura^{29,61}, T. Okusawa⁴⁵, N. Onda³³, N. Ospina²², L. Osu³⁶, N. Otani³³, Y. Oyama^{15,b}, V. Paolone⁴⁸, J. Pasternak²¹, D. Payne³⁷, M. Pfaff²¹, L. Pickering⁵⁸, B. Popov^{57,g}, A. J. Portocarrero Yrey¹⁵, M. Posiadala-Zezula⁶⁷, Y. S. Prabhu⁶⁷, H. Prasad⁷², F. Pupilli²⁴, B. Quilain^{28,36}

P. T. Quyen^{20,f}, E. Radicioni²², B. Radics⁷⁴ , M. A. Ramirez⁴⁷, R. Ramsden³¹, P. N. Ratoff³⁴, M. Reh⁶, G. Reina¹⁸, C. Riccio⁴³ , D. W. Riley¹³ , E. Rondio⁴², S. Roth⁵³ , N. Roy⁷⁴, A. Rubbia¹⁰ , L. Russo⁵⁷, A. Rychter⁶⁸, W. Saenz⁵⁷, K. Sakashita^{15,b}, S. Samani¹², F. Sánchez¹² , E. M. Sandford³⁷ , Y. Sato⁶⁴, T. Schefke³⁸ , C. M. Schloesser¹², K. Scholberg^{8,c} , M. Scott²¹, Y. Seiya^{45,h} , T. Sekiguchi^{15,b}, H. Sekiya^{29,60,c} , T. Sekiya⁶³, D. Seppala⁴⁰, D. Sgalaberna¹⁰, A. Shaikhiev²⁶, M. Shiozawa^{29,60}, Y. Shiraishi⁴⁴, A. Shvartsman²⁶, N. Skrobova²⁶ , K. Skwarczynski⁵² , D. Smyczek⁵³, M. Smy⁴, J. T. Sobczyk⁷², H. Sobel^{4,29} , F. J. P. Soler¹³ , A. J. Speers³⁴, R. Spina²², A. Srivastava¹⁸ , P. Stowell⁵⁵, Y. Stroke²⁶, I. A. Suslov³⁹, A. Suzuki³² , S. Y. Suzuki^{15,b}, M. Tada^{15,b}, S. Tairafune⁶⁰, A. Takeda⁶⁰, M. Takeuchi^{29,32} , K. Takeya⁴⁴, H. K. Tanaka^{60,c}, H. Tanigawa¹⁵, V. V. Tereshchenko³⁹, N. Thamm⁵³ , C. Touramanis³⁷ , N. Tran³³, T. Tsukamoto^{15,b}, M. Tzanov³⁸ , Y. Uchida²¹, M. Vagins^{4,29} , M. Varghese¹⁷ , I. Vasilyev³⁹, G. Vasseur⁵ , E. Villa^{11,12} , U. Virginet⁵⁷, T. Vladislavljjevic⁵⁸ , T. Wachala¹⁴, S.-i. Wada³², D. Wakabayashi⁶⁹, H. T. Wallace⁵⁵ , J. G. Walsh⁴⁰, L. Wan³, D. Wark^{46,58}, M. O. Wascko^{46,58} , A. Weber¹⁸ , R. Wendell³³, M. J. Wilking⁷⁹ , C. Wilkinson³⁵ , J. R. Wilson³¹ , K. Wood³⁵, C. Wret²¹ , J. Xia⁸⁰, K. Yamamoto^{45,h} , T. Yamamoto⁴⁵, C. Yanagisawa^{43,i}, Y. Yang⁴⁶ , T. Yano⁶⁰, N. Yershov²⁶, U. Yevarouskaya⁴³, M. Yokoyama^{59,c} , Y. Yoshimoto⁵⁹, Y. Yoshimura³³, R. Zaki⁷⁴, A. Zalewska¹⁴, J. Zalipska⁴², G. Zarnecki¹⁴ , J. Zhang^{66,80}, X. Y. Zhao¹⁰ , H. Zheng⁴³ , H. Zhong³², T. Zhu²¹, M. Ziembicki⁶⁸, E. D. Zimmerman⁶, M. Zito⁵⁷, S. Zsoldos³¹

¹ Department of Theoretical Physics, University Autonoma Madrid, 28049 Madrid, Spain

² Laboratory for High Energy Physics (LHEP), University of Bern, Albert Einstein Center for Fundamental Physics, Bern, Switzerland

³ Department of Physics, Boston University, Boston, Massachusetts, USA

⁴ Department of Physics and Astronomy, University of California, Irvine, Irvine, California, USA

⁵ IRFU, CEA, Université Paris-Saclay, 91191 Gif-sur-Yvette, France

⁶ Department of Physics, University of Colorado at Boulder, Boulder, Colorado, USA

⁷ Department of Physics, Colorado State University, Fort Collins, CO, USA

⁸ Department of Physics, Duke University, Durham, NC, USA

⁹ Department of Atomic Physics, Eötvös Loránd University, Budapest, Hungary

¹⁰ ETH Zurich, Institute for Particle Physics and Astrophysics, Zurich, Switzerland

¹¹ CERN European Organization for Nuclear Research, 1211 Genève 23, Switzerland

¹² University of Geneva, Section de Physique, DPNC, Geneva, Switzerland

¹³ School of Physics and Astronomy, University of Glasgow, Glasgow, UK

¹⁴ H. Niewodniczanski Institute of Nuclear Physics PAN, Cracow, Poland

¹⁵ High Energy Accelerator Research Organization (KEK), Tsukuba, Ibaraki, Japan

¹⁶ Department of Physics, University of Houston, Houston, TX, USA

¹⁷ Institut de Física d'Altes Energies (IFAE) - The Barcelona Institute of Science and Technology, Campus UAB, Bellaterra (Barcelona), Spain

¹⁸ Institut für Physik, Johannes Gutenberg-Universität Mainz, Staudingerweg 7, 55128 Mainz, Germany

¹⁹ IFIC (CSIC & University of Valencia), Valencia, Spain

²⁰ Institute For Interdisciplinary Research in Science and Education (IFIRSE), ICISE, Quy Nhon, Vietnam

²¹ Imperial College London, Department of Physics, London, UK

²² Dipartimento Interuniversitario di Fisica, INFN Sezione di Bari and Università e Politecnico di Bari, Bari, Italy

²³ Dipartimento di Fisica, INFN Sezione di Napoli and Università di Napoli, Naples, Italy

²⁴ Dipartimento di Fisica, INFN Sezione di Padova and Università di Padova, Padova, Italy

²⁵ INFN Sezione di Roma and Università di Roma "La Sapienza", Rome, Italy

²⁶ Institute for Nuclear Research of the Russian Academy of Sciences, Moscow, Russia

²⁷ International Centre of Physics, Institute of Physics (IOP), Vietnam Academy of Science and Technology (VAST), 10 Dao Tan, Ba Dinh, Hanoi, Vietnam

²⁸ ILANCE, CNRS - University of Tokyo International Research Laboratory, Kashiwa, Chiba 277-8582, Japan

²⁹ Kavli Institute for the Physics and Mathematics of the Universe (WPI), The University of Tokyo Institutes for Advanced Study, University of Tokyo, Kashiwa, Chiba, Japan

³⁰ Department of Physics, Keio University, Kanagawa, Japan

³¹ Department of Physics, King's College London, Strand, London WC2R 2LS, UK

³² Kobe University, Kobe, Japan

³³ Department of Physics, Kyoto University, Kyoto, Japan

³⁴ Physics Department, Lancaster University, Lancaster, UK

³⁵ Lawrence Berkeley National Laboratory, Berkeley, CA 94720, USA

³⁶ Ecole Polytechnique, IN2P3-CNRS, Laboratoire Leprince-Ringuet, Palaiseau, France

³⁷ Department of Physics, University of Liverpool, Liverpool, UK

³⁸ Department of Physics and Astronomy, Louisiana State University, Baton Rouge, LS, USA

³⁹ Joint Institute for Nuclear Research, Dubna, Moscow Region, Russia

⁴⁰ Department of Physics and Astronomy, Michigan State University, East Lansing, MI, USA

⁴¹ Department of Physics, Miyagi University of Education, Sendai, Japan

⁴² National Centre for Nuclear Research, Warsaw, Poland

⁴³ Department of Physics and Astronomy, State University of New York at Stony Brook, Stony Brook, New York, USA

- ⁴⁴ Department of Physics, Okayama University, Okayama, Japan
⁴⁵ Department of Physics, Osaka Metropolitan University, Osaka, Japan
⁴⁶ Department of Physics, Oxford University, Oxford, UK
⁴⁷ Department of Physics and Astronomy, University of Pennsylvania, Philadelphia, PA 19104, USA
⁴⁸ Department of Physics and Astronomy, University of Pittsburgh, Pittsburgh, Pennsylvania, USA
⁴⁹ School of Physics and Astronomy, Queen Mary University of London, London, UK
⁵⁰ Department of Physics, University of Regina, Regina, Saskatchewan, Canada
⁵¹ Department of Physics and Astronomy, University of Rochester, Rochester, NY, USA
⁵² Department of Physics, Royal Holloway University of London, Egham, Surrey, UK
⁵³ III. Physikalisches Institut, RWTH Aachen University, Aachen, Germany
⁵⁴ Departamento de Física Atómica, Molecular y Nuclear, Universidad de Sevilla, Sevilla 41080, Spain
⁵⁵ Department of Physics and Astronomy, University of Sheffield, Sheffield, UK
⁵⁶ Institute of Physics, University of Silesia, Katowice, Poland
⁵⁷ Laboratoire de Physique Nucléaire et de Hautes Energies (LPNHE), Sorbonne Université, Université Paris Diderot, CNRS/IN2P3, Paris, France
⁵⁸ STFC, Rutherford Appleton Laboratory, Harwell Oxford and Daresbury Laboratory, Warrington, UK
⁵⁹ Department of Physics, University of Tokyo, Tokyo, Japan
⁶⁰ Institute for Cosmic Ray Research, Kamioka Observatory, University of Tokyo, Kamioka, Japan
⁶¹ Institute for Cosmic Ray Research, Research Center for Cosmic Neutrinos, University of Tokyo, Kashiwa, Japan
⁶² Department of Physics, Tokyo Institute of Technology, Tokyo, Japan
⁶³ Department of Physics, Tokyo Metropolitan University, Tokyo, Japan
⁶⁴ Faculty of Science and Technology, Department of Physics, Tokyo University of Science, Noda, Chiba, Japan
⁶⁵ Department of Physics, University of Toronto, Toronto, ON, Canada
⁶⁶ TRIUMF, Vancouver, British Columbia, Canada
⁶⁷ Faculty of Physics, University of Warsaw, Warsaw, Poland
⁶⁸ Institute of Radioelectronics and Multimedia Technology, Warsaw University of Technology, Warsaw, Poland
⁶⁹ Faculty of Science, Department of Physics, Tohoku University, Miyagi, Japan
⁷⁰ Department of Physics, University of Warwick, Coventry, United Kingdom
⁷¹ Department of Physics, University of Winnipeg, Winnipeg, Manitoba, Canada
⁷² Faculty of Physics and Astronomy, Wrocław University, Wrocław, Poland
⁷³ Department of Physics, Yokohama National University, Yokohama, Japan
⁷⁴ Department of Physics and Astronomy, York University, Toronto, Ontario, Canada
⁷⁵ Department of Physics and Astronomy, Ghent University, Proeftuinstraat 86, 9000 Gent, Belgium
⁷⁶ South Dakota School of Mines and Technology, 501 East Saint Joseph Street, Rapid City, SD 57701, USA
⁷⁷ Department of Physics, University of Toyama, Toyama, Japan
⁷⁸ VNU University of Science, Vietnam National University, Hanoi, Vietnam
⁷⁹ School of Physics and Astronomy, University of Minnesota, Minneapolis, MI, USA
⁸⁰ SLAC National Accelerator Laboratory, Stanford University, Menlo Park, CA, USA

Received: 8 July 2025 / Accepted: 19 September 2025

© The Author(s) 2025

Abstract Bayesian analysis results require a choice of prior distribution. In long-baseline neutrino oscillation physics,

the usual parameterisation of the mixing matrix induces a prior that privileges certain neutrino mass and flavour state symmetries. Here we study the effect of privileging alternate symmetries on the results of the T2K experiment. We find that constraints on the level of CP violation (as given by the Jarlskog invariant) are robust under the choices of prior considered in the analysis. On the other hand, the degree of octant preference for the atmospheric angle depends on which symmetry has been privileged.

^a also at Université Paris-Saclay, Paris, France

^b also at J-PARC, Tokai, Japan

^c affiliated member at Kavli IPMU (WPI), the University of Tokyo, Japan

^d also at Moscow Institute of Physics and Technology (MIPT), Moscow region, Russia and National Research Nuclear University "MEPhI", Moscow, Russia

^e also at IPSA-DRII, Paris, France

^f also at the Graduate University of Science and Technology, Vietnam Academy of Science and Technology, Hanoi, Vietnam

^g also at JINR, Dubna, Russia

^h also at Nambu Yoichiro Institute of Theoretical and Experimental Physics (NITEP), Osaka, Japan

ⁱ also at BMCC/CUNY, Science Department, New York, New York, USA

^j also at Departament de Física de la Universitat Autònoma de Barcelona, Barcelona, Spain

^a e-mail: andres.lopezmoreno@lapp.in2p3.fr (corresponding author)

1 Introduction

Bayesian analyses have become powerful tools in accelerator long-baseline neutrino oscillation measurements [1, 2], due to their flexibility in incorporating non-Gaussian likelihood contributions, highly degenerate parameters, and post-analysis interpretation of results. However, in these Bayesian analyses, the choice of prior distribution may impact the

results, and understanding this effect of prior choice is important to interpreting them [3].

Neutrino oscillations are typically described using a unitary mixing matrix, U_{PMNS} , called the Pontecorvo-Maki-Nakagawa-Sakata (PMNS) matrix [4,5], using a common parameterisation, described in Sect. 2. The physical manifestation of neutrino oscillations depends only on the moduli of the matrix elements, yet the parameters in the common parameterisation are related in a non-trivial way to the physical observables $|U_{\alpha i}|^2$. This fact means that commonly used simple priors may not fully reflect the underlying physics or potential symmetries of the matrix.

This work explores the flavour symmetry biases induced by uniform priors on the parameters of the standard PMNS parameterisation, and investigates alternatives that bring out the flavour and mass symmetry preferences intrinsic to other parameterisations. The new priors are applied to T2K’s latest neutrino oscillation results [6] to quantify the robustness of its constraints. Section 2 develops a framework for finding useful alternate parameterisations, and Sect. 3 an interpretation of the parameterisations used in this analysis. Section 4 discusses the technique used to implement the new priors in T2K’s analysis and the uncertainties that arise with it. Finally, Sect. 5 reports the variations in T2K’s constraints induced by choosing a different prior.

2 Parameterisations of the leptonic mixing matrix

The standard parameterisation of the PMNS matrix, used in the Particle Data Group’s (PDG) summary [7], was inherited from the quark sector [8] and proved useful for describing early results in neutrino oscillation [9,10]. It represents the mixing matrix using three Tait-Bryan rotation angles [11] ($\theta_{12}, \theta_{23}, \theta_{13}$) and a complex phase δ_{CP} under the following construction [12]:

$$U_{PMNS} \equiv U_R = R_{23} \Gamma_\delta^\dagger R_{13} \Gamma_\delta R_{12}, \tag{1}$$

where, using the abbreviations $s_{ij} \equiv \sin \theta_{ij}$ and $c_{ij} \equiv \cos \theta_{ij}$,

$$\begin{aligned} R_{23} &\equiv \begin{pmatrix} 1 & 0 & 0 \\ 0 & c_{23} & s_{23} \\ 0 & -s_{23} & c_{23} \end{pmatrix} & R_{13} &\equiv \begin{pmatrix} c_{13} & 0 & s_{13} \\ 0 & 1 & 0 \\ -s_{13} & 0 & c_{13} \end{pmatrix} \\ R_{12} &\equiv \begin{pmatrix} c_{12} & s_{12} & 0 \\ -s_{12} & c_{12} & 0 \\ 0 & 0 & 1 \end{pmatrix} & \Gamma_\delta &\equiv \begin{pmatrix} e^{i\delta_{CP}} & 0 & 0 \\ 0 & 1 & 0 \\ 0 & 0 & 1 \end{pmatrix}. \end{aligned} \tag{2}$$

Since U_{PMNS} transforms from the mass to the flavour eigenstates, one can see that R_{12} acts directly on the mass basis and is therefore a rotation of the $(\nu_1 \nu_2)$ plane of mass states. Similarly, R_{23} acts on the flavour basis and is a rotation

of the $(\nu_\mu \nu_\tau)$ plane of flavour states. Finally, $\Gamma_\delta R_{13} \Gamma_\delta^\dagger$ is a rotation around the $(\nu_3 \nu_e)$ plane, involving both flavour and mass states.

This construction became the standard in neutrino oscillation analyses because when using it, the smallness of $|U_{e3}|$ and the hierarchical structure of the masses ($\Delta m_{21}^2 \ll \Delta m_{32}^2$) conspire to make the expressions for solar and atmospheric mixing surprisingly simple. For atmospheric neutrino energies and oscillation distances, the Δm_{32}^2 contribution dominates, and so we can approximate the oscillation probabilities as $\nu_\mu \leftrightarrow \nu_\tau$ mixing with a small contamination from ν_e . In the adiabatic MSW limit [13,14], solar experiments become a measurement of the ν_2 component projected onto ν_e . Moreover, $|U_{e3}|$ being small, ν_e survival can be studied as $\nu_1 \leftrightarrow \nu_2$ mixing with a small correction from a weakly mixed ν_3 state.

In the canonical (or standard) parameterisation¹ the angle θ_{23}^{PDG} (which defines R_{23}) mixes ν_μ with ν_τ and is a natural extension of the mixing angle in the 2-flavour atmospheric approximation. In the solar sector, the MSW resonance is very close to a direct measurement of the inner product $\langle \nu_e, \nu_2 \rangle (= |U_{e2}|)$, so a parameterisation that has U_{e2} as the simple element, written as $\sin \theta_{13} e^{-i\delta_{CP}}$, would be most optimal for solar experiments.² Instead, $|U_{e3}|$ is small enough to allow for the ν_1, ν_2 two-flavour approximation and makes the standard scheme convenient.

In general, one is free to choose the rotation axes for these Tait-Bryan rotations, and any set of perpendicular rotations will give rise to a valid parameterisation of the PMNS matrix. Although we have infinitely many choices, the only bases we have a reason to work with are the mass and flavour bases; therefore, we restrict ourselves to working with rotations defined around those. More formally, the infinite choices can be accessed by introducing additional U(3) rotations encoded in matrices X_1, X_2 to shift the axes to their desired positions

$$U_{PMNS} \equiv U_{X_1 X_2} = X_1 U_R X_2 \tag{3}$$

As long as X_i are not the identity, identical values for the angles θ_{ij} will lead to different matrices ($U_{X_1 X_2} \neq U_R$). If we want to describe the same neutrino mixing using the X and PDG forms of the PMNS matrix we must find two sets of mixing parameters $\theta_{ij}^{X_1 X_2}, \delta_{CP}^{X_1 X_2}$ and $\theta_{ij}^{PDG}, \delta_{CP}^{PDG}$ that fulfil $|U_{X_1 X_2}|_{\alpha k} = |U_{PDG}|_{\alpha k}$. That is, each choice of X_i gives rise to a new Tait-Bryan parameterisation which redefines the meaning of the mixing parameters.

We have discussed the origin of the canonical parameterisation in neutrino mixing and shown that there are many choices of Tait-Bryan parameterisations. Under no assump-

¹ Often referred to as the PDG parameterisation [15].

² We can identify the $\nu_\mu \nu_\tau / \nu_1 \nu_3$ parameterisation presented in section 2 as the matrix in question.

tions of hierarchy, these are all equivalent. In the next section, we motivate choices of particular Tait-Bryan parameterisations for oscillation analysis.

3 Choosing a parameterisation for Bayesian long-baseline oscillation analysis

Neutrino oscillation analyses are sensitive to the moduli of the elements of the PMNS matrix $|U_{\alpha i}|$, and a linear combination of the complex phases. To capture the unitary constraints, analysis tools use the standard parameters $(\theta_{12}, \theta_{23}, \theta_{13})$ and δ_{CP} instead. This presents a problem when choosing Bayesian priors: since the parameters are not physically motivated, there is no obvious correct choice for the prior distributions on the angles themselves, and it is precisely when making choices of priors over functions on the angles that choosing a parameterisation becomes important. Historically, T2K’s Bayesian framework used priors uniform on convenient expressions of the form $\sin^2 \theta_{i3}$ [16], which are proportional or closely related to leading order contributions of the angles to the oscillation probability.³ Since long-baseline experiments lack θ_{12} sensitivity but require a constraint on it to make precise measurements of CP-violation [17, 18], analysers are forced to impose a constraint on this angle. T2K uses the constraint from the global fit to solar and reactor measurements quoted by the PDG [19] as its $\sin^2 \theta_{12}$ prior.

Of additional note is the Jarlskog invariant, which can be written, $J_{CP} = s_{12}c_{12}s_{23}c_{23}s_{13}c_{13}^2 \sin \delta_{CP}$ [20], in the convention where θ_{13} is always the intermediate angle. It is of particular interest to experiments, as the value of J_{CP} governs CP violation in the lepton sector. J_{CP} is also useful when validating changes of parameterisation: its prior remains invariant for different Tait-Bryan parameterisations, as long as the priors on the mixing angles take the same form.

In a generic Tait-Bryan parameterisation as defined in expression 3, the R_{23} matrix is a rotation along the second and third states of some basis ν_a, ν_b, ν_c (in the standard parameterisation, this is the ν_e, ν_μ, ν_τ basis). On the other hand, R_{12} is a rotation of the first two states in some different basis ν_x, ν_y, ν_z (in the standard parameterisation, this is the ν_1, ν_2, ν_3 basis). These relations between the elements of a generic mixing matrix and its mixing parameters is portrayed in Fig. 1. A key takeaway from this construction is that the θ_{13} angle has a different relation to the moduli of the mixing matrix than θ_{12} and θ_{23} .

Now, consider priors uniform over the angles or, as is common in long-baseline analysis, over the square of the sines.

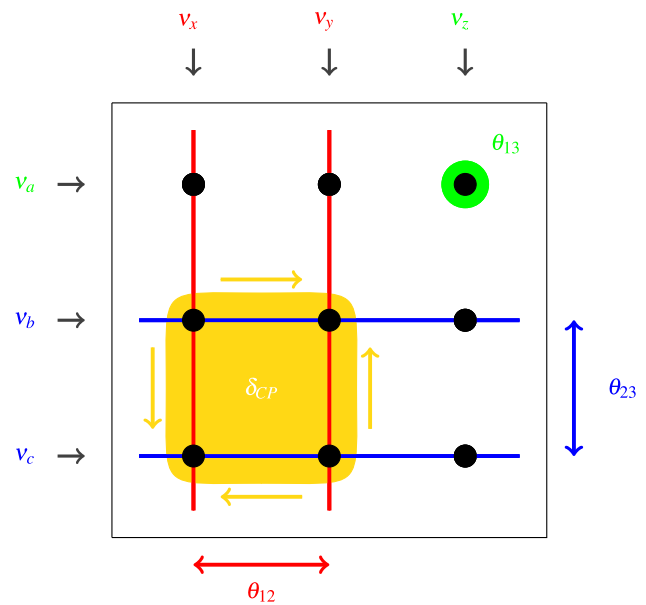


Fig. 1 Schematic of the mixing matrix generated by expanding $R_{23}\Gamma_\delta R_{13}\Gamma_\delta^\dagger R_{12}$ between the (ν_x, ν_y, ν_z) and (ν_a, ν_b, ν_c) bases. θ_{12} is a rotation that mixes the ν_x and ν_y columns (red), and θ_{23} is a rotation that mixes the ν_b and ν_c rows (blue). θ_{13} measures the magnitude of the only element untouched by the other angles (green). δ_{CP} governs the diagonality/anti-diagonality (indicated by the arrows) of the cofactor matrix to the θ_{13} element (yellow)

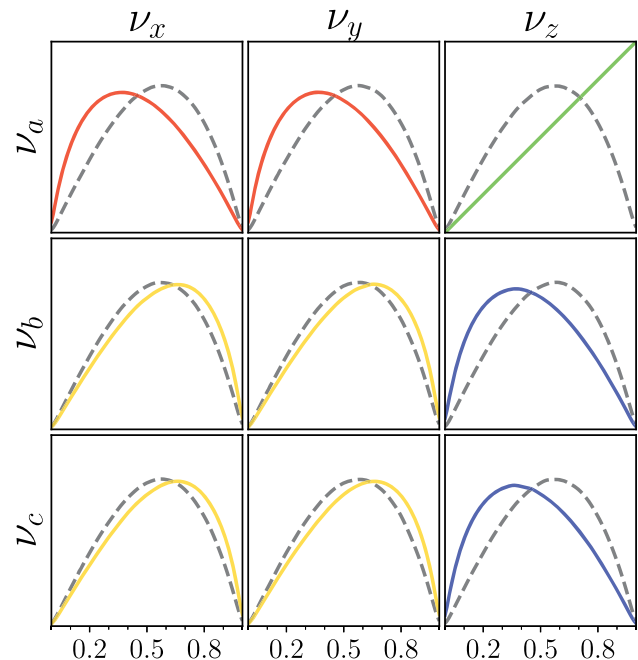


Fig. 2 Prior distributions on $|U_R|_{ij}$ resulting from uniform priors on $\sin^2 \theta_{ij}^X$ and δ_{CP}^X (solid lines) and expected distribution of $|U_R|_{ij}$ for random $U(3)$ matrices as given by the Haar measure (dashed lines). The upper-right distribution (governed by θ_{13}^X) breaks the 9-fold symmetry of the Haar-induced prior. The colours mirror the convention used in figure 1 to highlight the effect of the parameterisation

³ This is not the only choice of trigonometric function on the angles: other Bayesian oscillation fitters, such as NOvA’s, use priors defined on the square sines of the double angles[2]

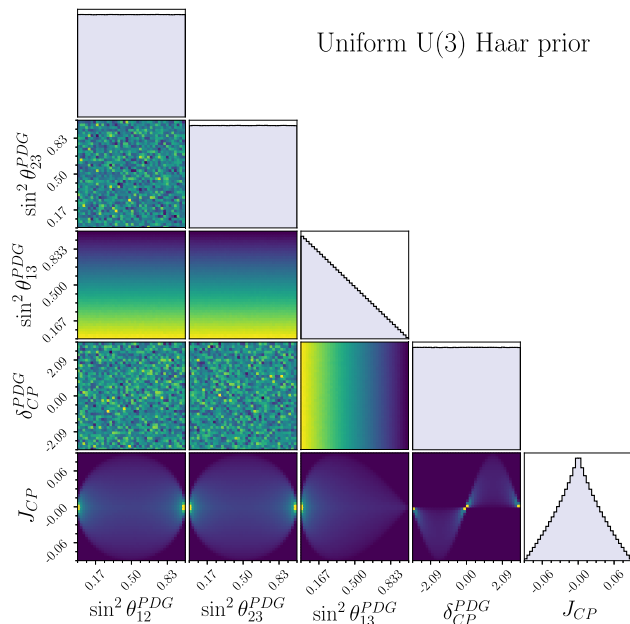


Fig. 3 1D and 2D marginalised priors on the standard parameters induced by the Haar measure of the U(3) matrix space. J_{CP} is the Jarlskog invariant and is not a free parameter

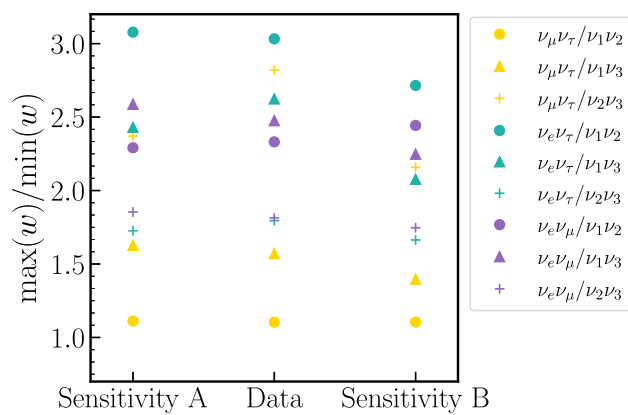


Fig. 4 Ratio of the largest over smallest weight applied to the MCMC chains when producing each prior. The ratios are small because the regions of parameter space which would receive the most extreme weights are excluded by the solar and/or T2K constraints. These ratios act as an upper bound for the amplification of the error in the MCMC approximation of the posterior due to the reweighing. The colors indicate the flavour pair of the prior and the shapes indicate the mass pair

These distributions induce uneven priors on the elements of the mixing matrix because not all elements are related to the mixing parameters in the same way: figure 2 shows the departure from the Haar distribution on the elements of the mixing matrix induced by setting uniform priors on the Tait-Bryan parameters. As hinted above, the largest deviation appears on the element most closely related to the θ_{13} angle, the only one that does not directly mix two states in the same basis.

Such priors (uniform in the $\sin^2 \theta_{ij}$ and δ_{CP} of the host parameterisation) will be referred to as Tait-Bryan priors, owing to the name of the parameterisation they are constructed on. These are interesting because they enable us to privilege flavour and mass symmetries, but to gauge their bias it is useful to compare them to a more general prior that lacks structural preferences. One good choice is the uniform prior in the Haar measure [21,22], which uses the topological group structure of U(3) to create an invariant volume element. The Haar prior corresponds to the distribution we should expect random unitary 3×3 matrices to follow, and is the natural choice if we assume the PMNS has no structural preferences. The hypothesis described by the Haar prior is commonly referred to as flavour anarchy [23], because it represents the antithesis to flavour hierarchies.

The Haar prior can be written in terms of the parameters of a Tait-Bryan parameterisation as uniform in the squared sines of the rotational angles $\sin^2 \theta_{12}$, $\sin^2 \theta_{23}$, uniform in the quartic cosine of the third angle $\cos^4 \theta_{13}$, and uniform in δ_{CP} ; its 1D and 2D projections onto the standard parameters are shown in Fig. 3, but one should keep in mind that these are correlated across the 4D parameter space. When written in terms of the elements of the mixing matrix, they all follow the same distribution $\pi_{\text{Haar}}(U_{ij}) = 4|U_{ij}|(1 - |U_{ij}|^2)$.

When compared to the flavour anarchic Haar prior, uniform priors in Tait-Bryan parameters tend to highlight symmetries between the rows and columns containing the states in the rotation planes of θ_{12} and θ_{23} . In particular, the canonical parameterisation induces a prior skewed towards ν_μ/ν_τ and ν_1/ν_2 symmetries. This is made apparent in Fig. 2, where the shape of the priors corresponds with the parameterisation-coded colouring from Fig. 1.

When attempting a Bayesian fit in long-baseline oscillation analysis, if the analyser strongly believes in a structureless mixing matrix, the correct prior is the Haar prior above. While there is no reason to believe in symmetries between random non-eigenstates, there is theoretical interest in exact and broken symmetries between mass states and flavour states [24–26]. We can find Tait-Bryan parameterisations whose uniform priors privilege each choice of flavour and mass symmetry by setting rotation planes that contain the desired states. This leads to 9 such parameterisations, one of which is the canonical scheme. Up to re-labelling of the angles and changing the sign of the complex phase, these 9 parameterisations can be arrived at by changing the combination and ordering of rotation matrices in Eq. 1 (see Appendix A). This method was used in [27] to arrive at the complete matrix expressions, which have been reproduced in Appendix A. Here we study the robustness of T2K’s latest results [6] under priors derived from these 8 additional parameterisations.

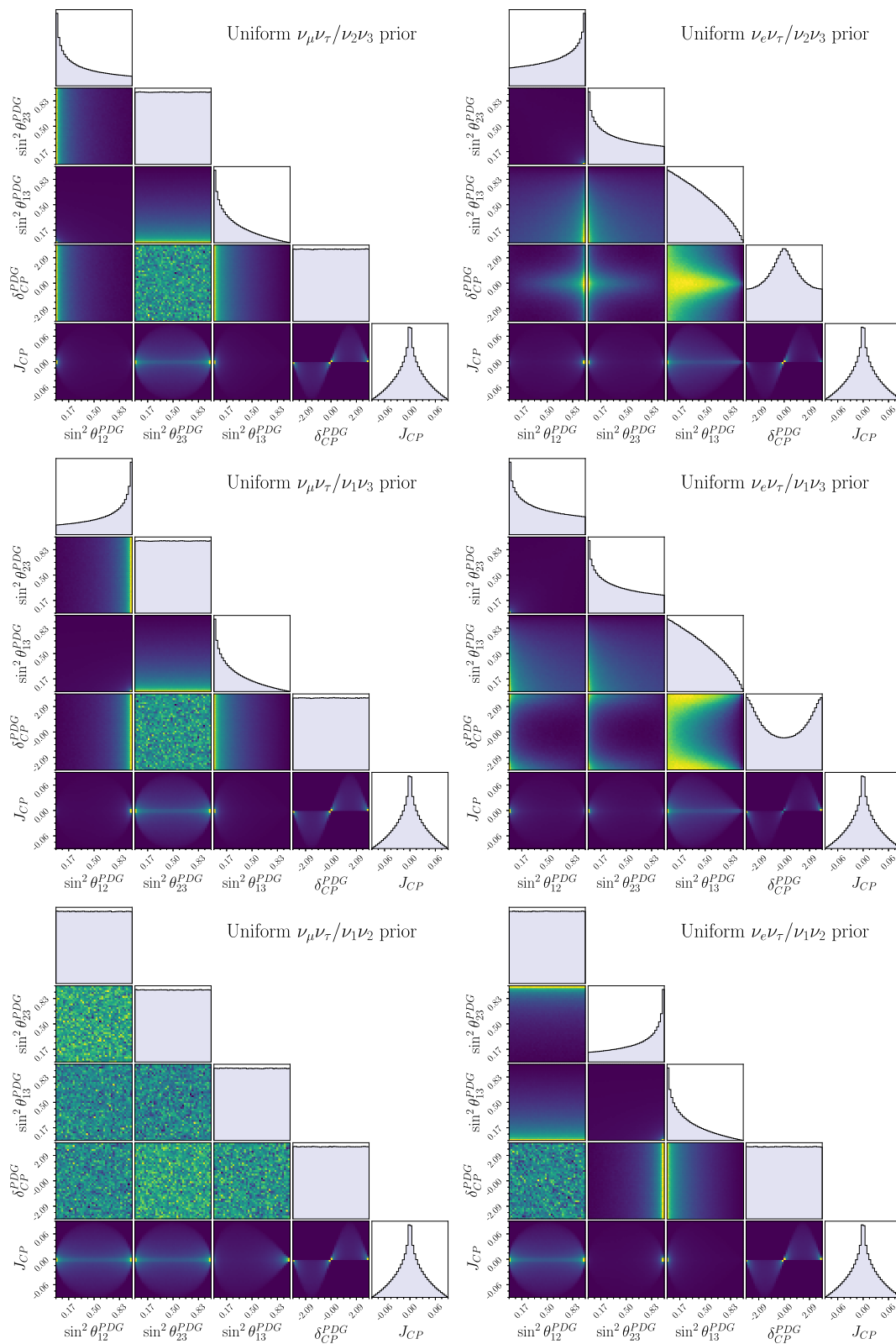


Fig. 5 Marginalised 1D and 2D Tait-Bryan priors over the standard parameters. Each prior was generated by drawing uniformly in some alternate Tait-Bryan parameterisation (labelled by the symmetry they privilege). The bottom-left plot on the first page corresponds to the standard parameterisation (here labelled as $\nu_\mu\nu_\tau/\nu_1\nu_2$) and is there-

fore flat everywhere. The plots are arranged in groups of three (left and right columns on the first page, three plots on the second page) by the flavour symmetry they privilege. Supplementary material displays the nine plots according to the symmetries they privilege, and gives an intuition on how to interpret the priors

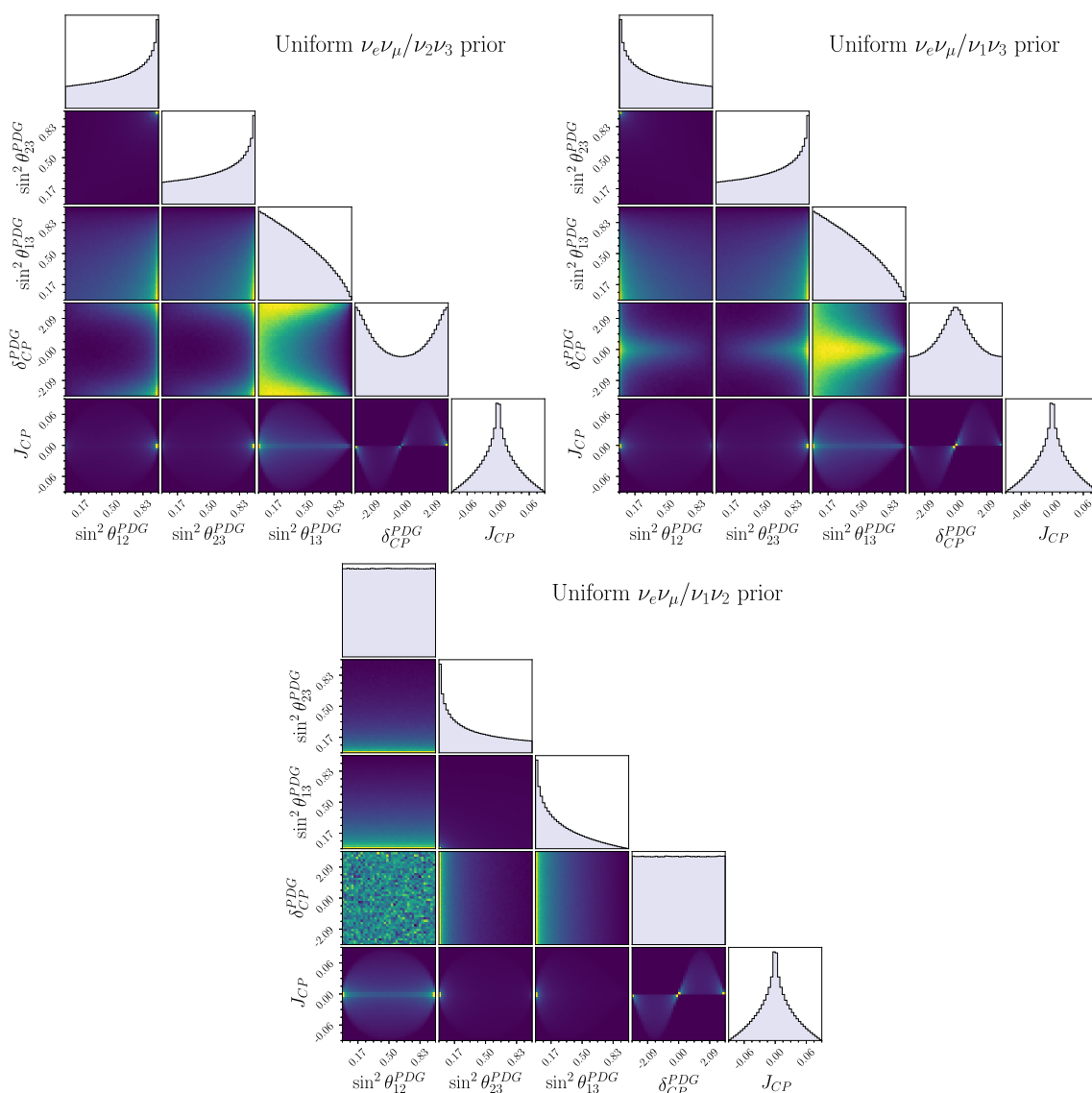


Fig. 5 continued

4 MCMC fits in alternate parameterisations

The reanalysis of T2K's results is performed by weighting steps from a Markov chain Monte Carlo (MCMC) analysis of T2K data, as rerunning the analysis is computationally expensive. To do this, the ratio between the prior used in the original analysis and the new priors is calculated and the posterior distributions are reweighted accordingly. While there is an analytic bijective map between the parameterisations, propagating the alternate prior distributions onto the standard parameters analytically is a challenging and time-consuming task. Instead, the weights are approximated numerically on a grid. This approximation is performed through the binned distribution in the original space of a large (10^{11} draws) uni-

formly distributed sample drawn from the alternate parameterisation space.

This method introduces two sources of uncertainty: statistical uncertainties in the weight approximation, which become negligible in areas of high posterior density,⁴ and amplified uncertainties resulting from giving a large weight to a sparsely populated posterior bin.

Assuming the approximated weights and the posterior bins follow Poisson distributions and the number of steps in any two posterior bins are uncorrelated, the induced uncertainty

⁴ This is true as long as the assigned weights for steps in the same posterior bin are largely uncorrelated. We ensure this is the case by having many more grid points than steps in our Markov-Chain and studying marginalised 1D and 2D posteriors instead of the complete 4D posterior distribution.

on the number of steps n in bin b of the reweighted posterior $\text{Var}(n(b))$ is

$$\text{Var}(n(b)) = \frac{N}{W} w(b)p(b) + \frac{N^2}{W} w(b)p^2(b) + Nw^2(b)p(b) \tag{4}$$

where N is the total number of steps in the MCMC chain, W is the number of draws used in the approximation of the weights, $w(b)$ is the true weight of bin b and $p(b)$ is the true value of the unweighted posterior at bin b .

The first two terms can be made arbitrarily small by taking a large sample in the calculation of the weights; in this study, their contribution is kept at below 1% of the original bin uncertainty for the entire 3σ range. We can find an upper bound for the final term by assuming the largest weights are given to the low posterior density regions and the smallest weights are assigned to the highest posterior density bins. In this scenario, the final term is at most

$$\sqrt{Nw^2(b)p(b)} \leq \frac{\max(w(b'))}{\min(w(b'))} \sqrt{Np(b)} \tag{5}$$

that is, the ratio of largest to smallest weight applied to an MCMC chain serves as a (conservative) upper bound for the amplification factor on the variance of the posterior approximation introduced by the new weights.

Figure 4 shows the ratio between the largest and smallest applied weights of each parameterisation for two sensitivity analyses and one data chain.⁵ Taking the largest ratio as an upper limit of the amplification, the new uncertainty is at most 3 times larger than the original; this is satisfactory because the statistical uncertainty within the 3σ region of our 2×10^8 step posterior chains is sub-percent.

5 Results

Figure 5 shows the 1D and 2D marginalised priors derived from uniform priors in the alternate parameterisations on the standard parameters. Some parameterisations share a uniform prior on δ_{CP}^{PDG} while others favour small/large δ_{CP} by up to 15%. This is the consequence of a re-definition of the complex phase happening in those parameterisations where the elements with a complex component swap places with the purely real ones.⁶ Since J_{CP} takes the same from under all parameterisations, every Tait-Bryan prior must assign to

⁵ The oscillation parameters used in the sensitivity fits are presented in Appendix B.

⁶ This is allowed because oscillations are only sensitive to specific linear combinations of the phases.

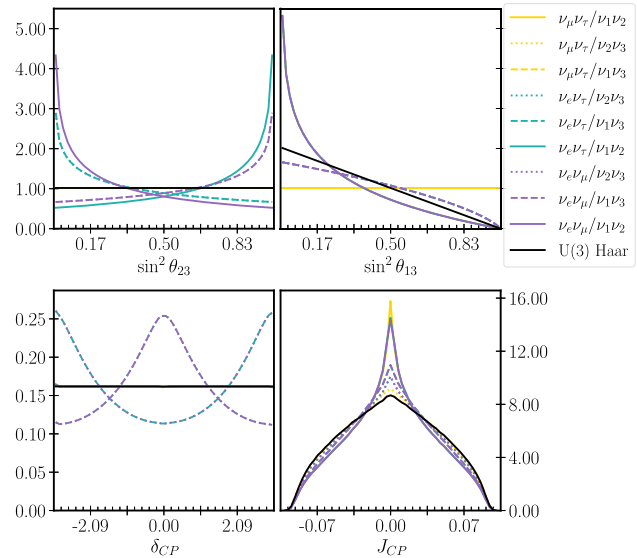


Fig. 6 Priors uniform in each of the 9 flavour/mass symmetric Tait-Bryan parameterisations and Haar prior for the relevant oscillation parameters, after imposing a Gaussian prior on $\sin^2 \theta_{12}^{\text{PDG}}$ ($\mu = 0.307, \sigma = 0.041$) derived from the θ_{12} constraint reported by the PDG. The priors are labelled by the symmetries they privilege, and the standard PDG prior is $\nu_\mu \nu_\tau / \nu_1 \nu_2$. The colours indicate the flavour pair of the prior, and the line styles indicate the mass pair. Since some parameterisations share the same row or column symmetry, the lines often overlap. The y-axis is normalised to the standard uniform prior

it the same distribution. This is precisely what our computation shows, and serves as a sanity check when changing parameterisations.

We apply the solar constraint by imposing a Gaussian prior on $\sin^2 \theta_{12}^{\text{PDG}}$ taken from the global solar constraint in the PDG report [19] (as is usual in T2K analyses). Doing so on top of uniform priors on each parameterisation breaks the invariance and leads to different prior distributions on the amount of CP violation. This is evident in Fig. 6, where the alternate parameterisation priors have been applied together with the solar constraint.

In future oscillation analyses, to more accurately capture the solar measurement and remove prior reliance on the smallness of $|U_{e3}|$, it is advisable to consider alternative solar constraints. This could be achieved by using priors derived from KamLAND’s reactor measurements [28] or by playing the reparameterisation game to express the solar measurement in a Tait-Bryan scheme where the simple element falls in U_{e2} .

Figures 7 and 8 show the 1D and 2D marginalised posteriors resulting from applying the Tait-Bryan priors, together with the solar constraint, to T2K’s latest oscillation analysis [6]. Although the priors vary significantly (Fig. 6), the credible regions show only small variations from the original fit.

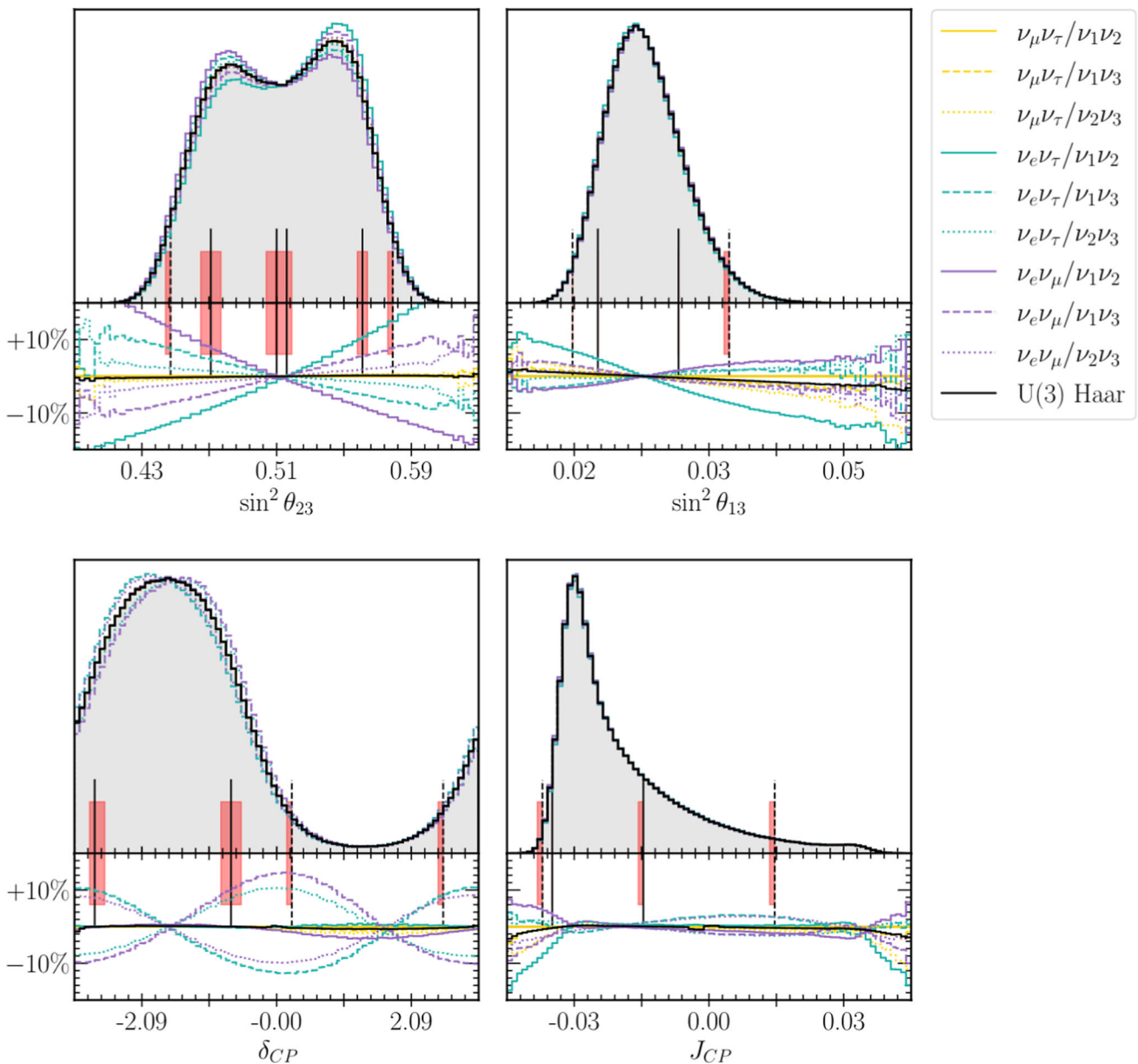


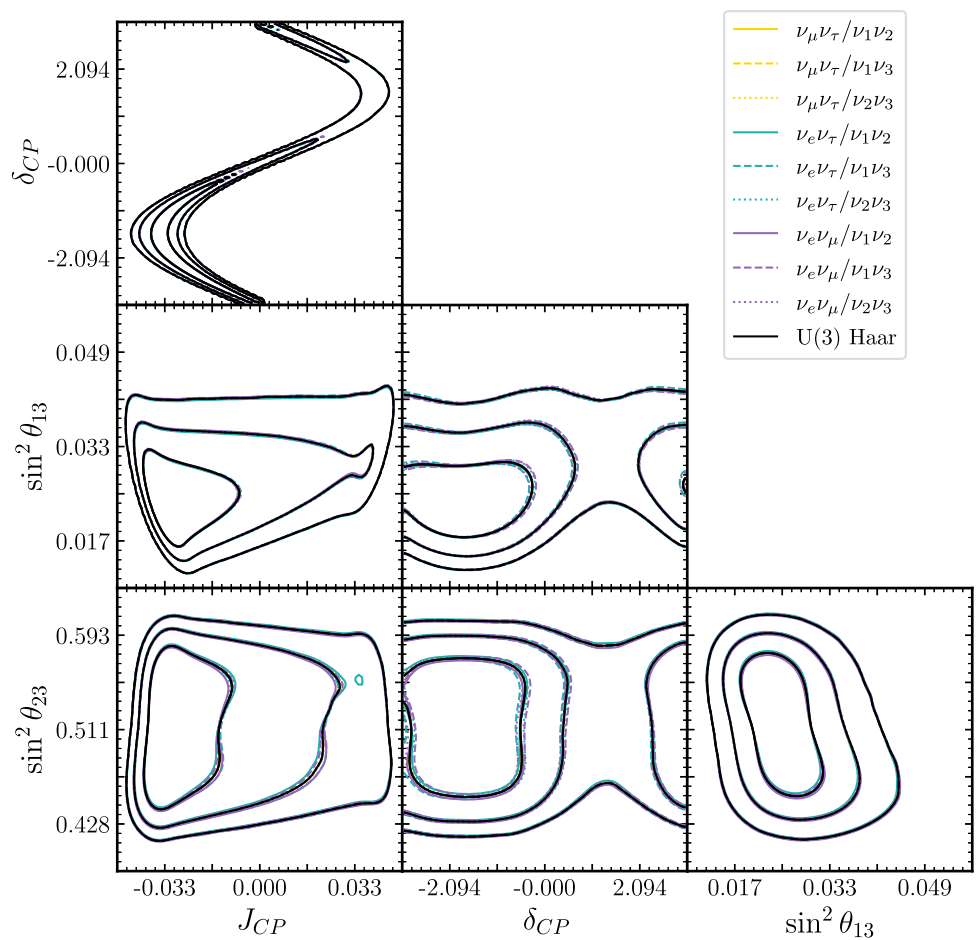
Fig. 7 1D marginalised posterior over the standard parameters of T2K’s 2022 oscillation analysis, reweighted under the 9 flavour/mass symmetry and Haar priors. The colours indicate the flavour pair of the prior and the line styles indicate the mass pair. The grey area corresponds to the original posterior generated using the PDG prior, and the vertical

lines mark the 1σ (filled) and 2σ (dashed) credible regions. The red areas include the boundaries of the credible intervals for all the studied priors, and serve as an indication of how much each interval varies. The bottom plot shows the fractional bin change from the standard prior

A particularly interesting way to quantify the prior dependence on T2K’s physics conclusions is to ask how it affects the credible intervals. Despite the fractional bin-by-bin differences being up to $\approx 10\%$, meaningful variations in the intervals only appear in the $\sin^2 \theta_{23}^{\text{PDG}}$ posteriors. In this latter case, several alternate priors result in an enhancement of the posterior in the lower octant, indicating that the weak upper-octant preference of the original analysis is affected by the choice of prior.

In terms of CP-violation, while the marginalised posteriors in δ_{CP} show some variation, the credible intervals over the Jarlskog invariant stay effectively constant. Since it is more closely related to the experimental event rates than the mixing angles [29], it is not surprising to see that the data imposes more robust constraints on J_{CP} than on the individual mixing parameters. This serves as a reminder that the Jarlskog invariant is the true measure of CP-violation and δ_{CP} constraints do not give the full picture and shows that

Fig. 8 2D marginalised posteriors for T2K’s 2022 oscillation analysis, reweighted under the 9 flavour/mass symmetry and Haar priors. The contour lines correspond to the 1σ , 2σ , and 3σ credible regions, and often overlap



T2K’s evidence for CP violation is robust under these choices of prior.

Appendix B presents the results from running this same analysis on two additional MCMC posteriors which come from sensitivity analyses. The simulated data for the Asimov A MCMC chain were generated using parameter values similar to T2K’s best fit, and serve to confirm that these results are not an artefact of some undetected tensions between T2K samples. The Asimov B MCMC chain uses vastly different parameter values (though still consistent with existing data) and serves to verify that the small difference in the posteriors is a consequence of T2K’s strong constraining power and not an artefact of the region of parameter space favoured by current data.

6 Conclusion

This work discussed the space of Tait-Bryan parameterisations of the lepton mixing matrix and their relation to row-column symmetries. We showed that uniform priors in the parameters of the standard PMNS parameterisation privilege symmetries between the $\nu_{\mu(1)}$ and $\nu_{\tau(2)}$ flavour (mass) neutrino eigenstates and constructed a set of nine parameterisations that capture all such flavour and mass symmetries.

We presented a method for applying priors induced by these parameterisations to Bayesian long-baseline neutrino oscillation analysis and discussed the additional uncertainties introduced by this process. Finally, we studied the changes to T2K’s latest constraints arising from choosing the new priors. We found no significant alterations to the results on CP violation in neutrino oscillations; still, the current slight preference for the upper octant is sensitive to the choice of prior, and almost vanishes under some of these alternate constraints.

Acknowledgements We thank the J-PARC staff for superb accelerator performance. We thank the CERN NA61/SHINE Collaboration for providing valuable particle production data. We acknowledge the support of MEXT, JSPS KAKENHI (JP16H06288, JP18K03682, JP18H03701, JP18H05537, JP19J01119, JP19J22440, JP19J22258, JP20H00162, JP20H00149, JP20J20304) and bilateral programs (JPJSBP120204806, JPJSBP120209601), Japan; NSERC, the NRC, and CFI, Canada; the CEA and CNRS/IN2P3, France; the DFG (RO 3625/2), Germany; the NKFIH (NKFIH 137812 and TKP2021-NKTA-64), Hungary; the INFN, Italy; the Ministry of Education and Science(2023/WK/04) and the National Science Centre (UMO-2018/30/E/ST2/00441 and UMO-2022/46/E/ST2/00336), Poland; the RSF19-12-00325, RSF22-12-00358, Russia; MICINN (SEV-2016-0588, PID2019-107564GB-I00, PGC2018-099388-BI00, PID2020-114687GB-I00) Government of Andalucia (FQM160, SOMM17/6105/UGR) and the University of

Tokyo ICRR’s Inter-University Research Program FY2023 Ref. J1, and ERDF funds and CERCA program, Spain; the SNSF and SERI (200021_185012, 200020_188533, 20FL21_186178I), Switzerland; the STFC and UKRI, UK; and the DOE, USA. We also thank CERN for the UA1/NOMAD magnet, DESY for the HERA-B magnet mover system, the BC DRI Group, Prairie DRI Group, ACENET, SciNet, and CalculQuebec consortia in the Digital Research Alliance of Canada, GridPP and the Emerald High Performance Computing facility in the United Kingdom, and the CNRS/IN2P3 Computing Center in France. In addition, the participation of individual researchers and institutions has been further supported by funds from the ERC (FP7), “la Caixa” Foundation (ID 100010434, fellowship code LCF/BQ/IN17/11620050), the European Union’s Horizon 2020 Research and Innovation Programme under the Marie Skłodowska-Curie grant agreement numbers 713673 and 754496, and H2020 grant numbers RISE-GA822070-JENNIFER2 2020 and RISE-GA872549-SK2HK; the JSPS, Japan; the Royal Society, UK; French ANR grant number ANR-19-CE31-0001; the SNF Eccellenza grant number PCEFP2_203261; and the DOE Early Career programme, USA. For the purposes of open access, the authors have applied a Creative Commons Attribution licence to any Author Accepted Manuscript version arising.

Data Availability Statement Data will be made available on reasonable request. [Author’s comment: Data cannot be made available for reasons disclosed in the data availability statement].

Code Availability Statement Code/software will be made available on reasonable request. [Author’s comment: A zenodo permalink with a python release was sent to the editor.]

Open Access This article is licensed under a Creative Commons Attribution 4.0 International License, which permits use, sharing, adaptation, distribution and reproduction in any medium or format, as long as you give appropriate credit to the original author(s) and the source, provide a link to the Creative Commons licence, and indicate if changes were made. The images or other third party material in this article are included in the article’s Creative Commons licence, unless indicated otherwise in a credit line to the material. If material is not included in the article’s Creative Commons licence and your intended use is not permitted by statutory regulation or exceeds the permitted use, you will need to obtain permission directly from the copyright holder. To view a copy of this licence, visit <http://creativecommons.org/licenses/by/4.0/>.
Funded by SCOAP³.

Appendix A Expanded forms of the PMNS matrix in 9 rotation parameterisations

Here we present the full form of the PMNS matrix under the 9 (6 Tait-Bryan and 3 Euler rotations) parameterisations considered in this analysis. Up to relabeling of the mixing angles and sign of the complex phase, six of these are equivalent to the parameterisations derived in [27] by considering different products of the matrices R_{23} , $\Gamma_\delta^\dagger R_{13} \Gamma_\delta$, and R_{12} . For example, $U_{\nu_\mu \nu_\tau / \nu_1 \nu_3} \equiv P_\parallel \times U_R \times P_-$ is structurally equivalent to the Tait-Bryan rotation $R_{23} \times R_{12} \times \Gamma_\delta^\dagger \times R_{13} \times \Gamma_\delta$. Using the construction below, the intrinsic flavour and mass symmetries of each parameterisation become more obvious. The ordering of the parameterisations mirrors the label in Fig. 7, and expression A.1 is the canonical form. The correspondences with the parameterisations in [27] may be identified by spotting the position of the single-angle element. The 9 matrices are generated by identifying X_1 and X_2 with one of the three 3×3 even permutation matrices (i.e. the action of the alternating group A_3):

$$P_\parallel = \begin{pmatrix} 1 & 0 & 0 \\ 0 & 1 & 0 \\ 0 & 0 & 1 \end{pmatrix}, \quad P_+ = \begin{pmatrix} 0 & 1 & 0 \\ 0 & 0 & 1 \\ 1 & 0 & 0 \end{pmatrix}, \quad P_- = \begin{pmatrix} 0 & 0 & 1 \\ 1 & 0 & 0 \\ 0 & 1 & 0 \end{pmatrix}.$$

$$U_{\nu_\mu \nu_\tau / \nu_1 \nu_2} = P_\parallel \times U_R \times P_\parallel = \begin{pmatrix} c_{12}c_{13} & s_{12}c_{13} & s_{13}e^{-i\delta_{CP}} \\ -s_{12}c_{23} - c_{12}s_{23}s_{13}e^{i\delta_{CP}} & c_{12}c_{23} - s_{12}s_{23}s_{13}e^{i\delta_{CP}} & s_{23}c_{13} \\ s_{12}s_{23} - c_{12}c_{23}s_{13}e^{i\delta_{CP}} & -c_{12}s_{23} - s_{12}c_{23}s_{13}e^{i\delta_{CP}} & c_{23}c_{13} \end{pmatrix} \quad (A.1)$$

$$U_{\nu_\mu \nu_\tau / \nu_2 \nu_3} = P_\parallel \times U_R \times P_+ = \begin{pmatrix} s_{13}e^{-i\delta_{CP}} & c_{12}c_{13} & s_{12}c_{13} \\ s_{23}c_{13} & -s_{12}c_{23} - c_{12}s_{23}s_{13}e^{i\delta_{CP}} & c_{12}c_{23} - s_{12}s_{23}s_{13}e^{i\delta_{CP}} \\ c_{23}c_{13} & s_{12}s_{23} - c_{12}c_{23}s_{13}e^{i\delta_{CP}} & -c_{12}s_{23} - s_{12}c_{23}s_{13}e^{i\delta_{CP}} \end{pmatrix} \quad (A.2)$$

$$U_{\nu_\mu \nu_\tau / \nu_1 \nu_3} = P_\parallel \times U_R \times P_-$$

$$= \begin{pmatrix} c_{12}c_{13} & s_{13}e^{-i\delta_{CP}} & s_{12}c_{13} \\ -s_{12}c_{23} - c_{12}s_{23}s_{13}e^{i\delta_{CP}} & s_{23}c_{13} & c_{12}c_{23} - s_{12}s_{23}s_{13}e^{i\delta_{CP}} \\ s_{12}s_{23} - c_{12}c_{23}s_{13}e^{i\delta_{CP}} & c_{23}c_{13} & -c_{12}s_{23} - s_{12}c_{23}s_{13}e^{i\delta_{CP}} \end{pmatrix} \tag{A.3}$$

$$U_{\nu_e\nu_\tau/\nu_1\nu_2} = P_- \times U_R \times P_{\mathbb{I}} \\ = \begin{pmatrix} -s_{12}c_{23} - c_{12}s_{23}s_{13}e^{i\delta_{CP}} & c_{12}c_{23} - s_{12}s_{23}s_{13}e^{i\delta_{CP}} & s_{23}c_{13} \\ c_{12}c_{13} & s_{12}c_{13} & s_{13}e^{-i\delta_{CP}} \\ s_{12}s_{23} - c_{12}c_{23}s_{13}e^{i\delta_{CP}} & -c_{12}s_{23} - s_{12}c_{23}s_{13}e^{i\delta_{CP}} & c_{23}c_{13} \end{pmatrix} \tag{A.4}$$

$$U_{\nu_e\nu_\tau/\nu_2\nu_3} = P_+ \times U_R \times P_- \\ = \begin{pmatrix} s_{23}c_{13} & -s_{12}c_{23} - c_{12}s_{23}s_{13}e^{i\delta_{CP}} & c_{12}c_{23} - s_{12}s_{23}s_{13}e^{i\delta_{CP}} \\ s_{13}e^{-i\delta_{CP}} & c_{12}c_{13} & s_{12}c_{13} \\ c_{23}c_{13} & s_{12}s_{23} - c_{12}c_{23}s_{13}e^{i\delta_{CP}} & -c_{12}s_{23} - s_{12}c_{23}s_{13}e^{i\delta_{CP}} \end{pmatrix} \tag{A.5}$$

$$U_{\nu_e\nu_\tau/\nu_1\nu_3} = P_- \times U_R \times P_- \\ = \begin{pmatrix} -s_{12}c_{23} - c_{12}s_{23}s_{13}e^{i\delta_{CP}} & s_{23}c_{13} & c_{12}c_{23} - s_{12}s_{23}s_{13}e^{i\delta_{CP}} \\ c_{12}c_{13} & s_{13}e^{-i\delta_{CP}} & s_{12}c_{13} \\ s_{12}s_{23} - c_{12}c_{23}s_{13}e^{i\delta_{CP}} & c_{23}c_{13} & -c_{12}s_{23} - s_{12}c_{23}s_{13}e^{i\delta_{CP}} \end{pmatrix} \tag{A.6}$$

$$U_{\nu_e\nu_\mu/\nu_1\nu_2} = P_+ \times U_R \times P_{\mathbb{I}} \\ = \begin{pmatrix} -s_{12}c_{23} - c_{12}s_{23}s_{13}e^{i\delta_{CP}} & c_{12}c_{23} - s_{12}s_{23}s_{13}e^{i\delta_{CP}} & s_{23}c_{13} \\ s_{12}s_{23} - c_{12}c_{23}s_{13}e^{i\delta_{CP}} & -c_{12}s_{23} - s_{12}c_{23}s_{13}e^{i\delta_{CP}} & c_{23}c_{13} \\ c_{12}c_{13} & s_{12}c_{13} & s_{13}e^{-i\delta_{CP}} \end{pmatrix} \tag{A.7}$$

$$U_{\nu_e\nu_\mu/\nu_2\nu_3} = P_+ \times U_R \times P_+ \\ = \begin{pmatrix} s_{23}c_{13} & -s_{12}c_{23} - c_{12}s_{23}s_{13}e^{i\delta_{CP}} & c_{12}c_{23} - s_{12}s_{23}s_{13}e^{i\delta_{CP}} \\ c_{23}c_{13} & s_{12}s_{23} - c_{12}c_{23}s_{13}e^{i\delta_{CP}} & -c_{12}s_{23} - s_{12}c_{23}s_{13}e^{i\delta_{CP}} \\ s_{13}e^{-i\delta_{CP}} & c_{12}c_{13} & s_{12}c_{13}e^{-i\delta_{CP}} \end{pmatrix} \tag{A.8}$$

$$U_{\nu_e\nu_\mu/\nu_1\nu_3} = P_+ \times U_R \times P_- \\ = \begin{pmatrix} -s_{12}c_{23} - c_{12}s_{23}s_{13}e^{i\delta_{CP}} & s_{23}c_{13} & c_{12}c_{23} - s_{12}s_{23}s_{13}e^{i\delta_{CP}} \\ s_{12}s_{23} - c_{12}c_{23}s_{13}e^{i\delta_{CP}} & c_{23}c_{13} & -c_{12}s_{23} - s_{12}c_{23}s_{13}e^{i\delta_{CP}} \\ c_{12}c_{13} & s_{13}e^{-i\delta_{CP}} & s_{12}c_{13} \end{pmatrix} \tag{A.9}$$

Table 1 Parameter values for Asimov fits in the T2K experiment

Parameter	Asimov A value	Asimov B value
$\sin^2 \theta_{12}^{\text{PDG}}$	0.307	0.307
$\sin^2 \theta_{23}^{\text{PDG}}$	0.561	0.45
$\sin^2 \theta_{13}^{\text{PDG}}$	0.022	0.022
δ_{CP}^{PDG}	-1.601	0
Δm_{21}^2	$2.494 \times 10^{-3} \text{ eV}^2$	$2.494 \times 10^{-3} \text{ eV}^2$
Δm_{32}^2	$7.53 \times 10^{-5} \text{ eV}^2$	$7.53 \times 10^{-5} \text{ eV}^2$

space, we run the same analysis on chains generated from two Asimov datasets [30] at points Asimov A and Asimov B of the phase space (defined in Table 1). Asimov A is chosen to recreate posteriors similar to the data fit, and Asimov B is chosen to represent a scenario with no CP violation and true lower octant.

Figures 9 and 10 show the 1D marginalised posteriors for Asimov points A and B, and reweighted with the Tait-Bryan priors. The results are consistent with the conclusions of section 5: the θ_{23} octant preference weakens for some priors but the constraints remain largely the same. Although the posteriors for δ_{CP} vary substantially (Asimov B experiences a shift of the highest posterior density from 0 to $\pm\pi$), the constraints on the amount of CP violation as given by the Jarlskog invariant show sub-percent change within the 2σ range. This falls in line with the fact that T2K has good sensitivity to the observable J_{CP} , which is a more robust measure of CP-violation than a prior-dependent extraction to δ_{CP} .

Appendix B Fake data results

To test whether the main results in section 5 are due to the robustness of T2K’s constraining power or due to the particular shape of the likelihood in the favoured area of parameter

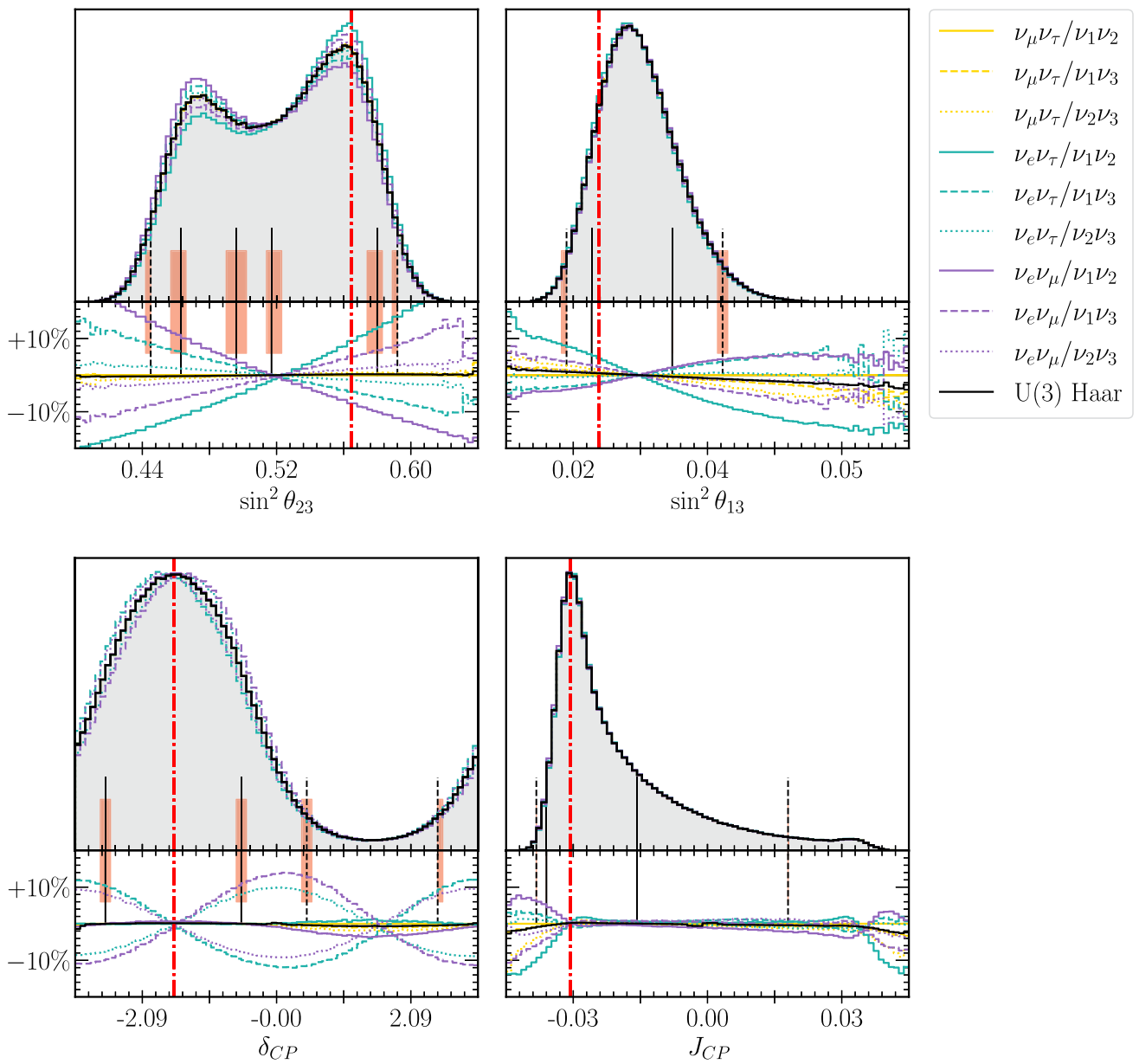


Fig. 9 1D marginalised posterior over the standard parameters of a T2K Asimov A fit, reweighted under the 9 flavour/mass symmetry and Haar priors. The black line corresponds to the original posterior generated using the PDG prior, and the vertical lines mark the 1σ (filled) and

2σ (dashed) credible regions. The bottom plot shows the fractional bin change from the standard prior. The Asimov point is marked with a red line

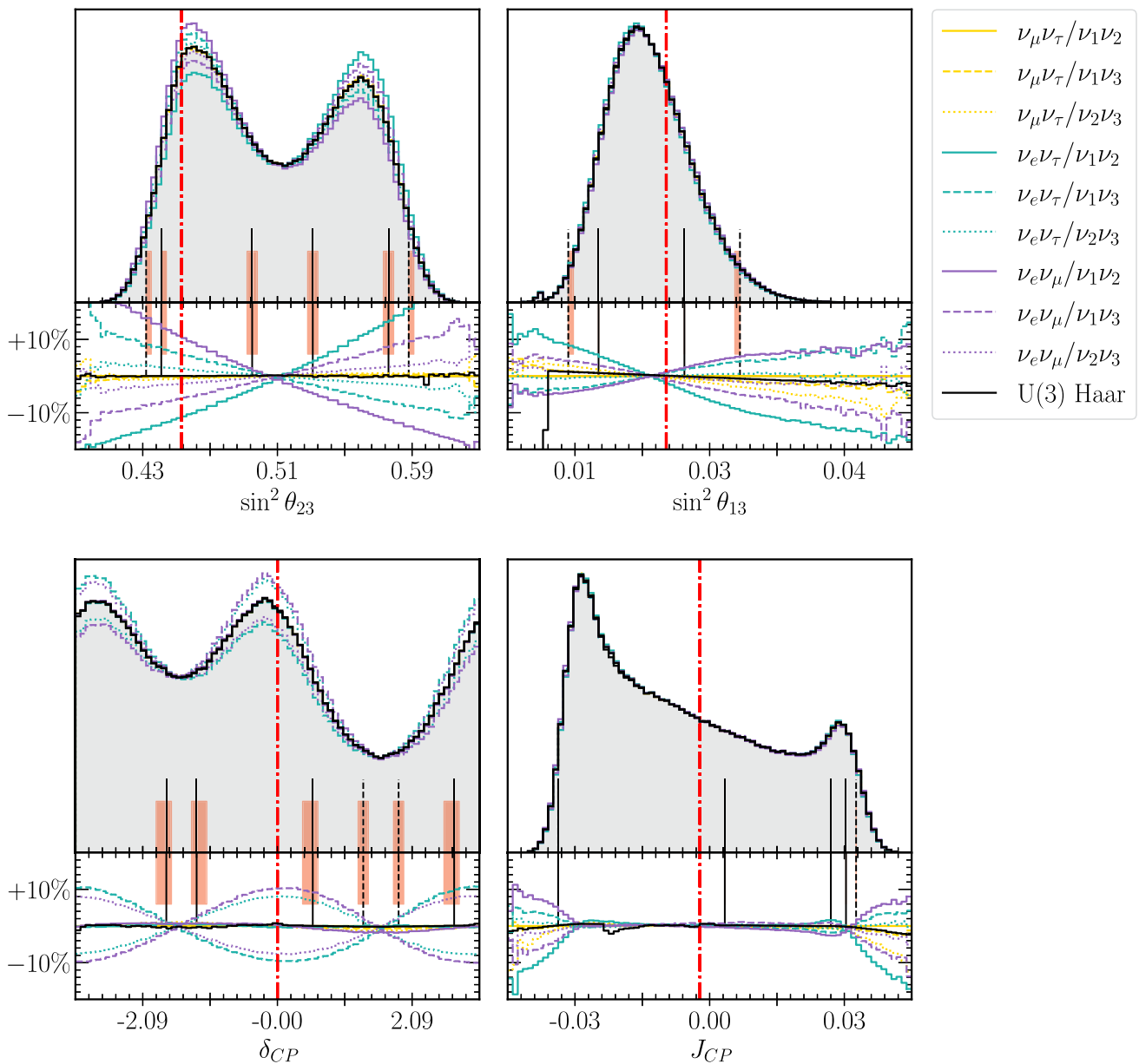


Fig. 10 1D marginalised posterior over the standard parameters of a T2K Asimov B fit, reweighted under the 9 flavour/mass symmetry and Haar priors. The black line corresponds to the original posterior generated using the PDG prior, and the vertical lines mark the 1σ (filled) and

2σ (dashed) credible regions. The bottom plot shows the fractional bin change from the standard prior. The Asimov point is marked with a red line

Appendix C Data release

This study further analyses the results reported in [31], which provides the associated data. A small Python package facilitating transformations between the parameterisations used in this work is available at <https://zenodo.org/records/17458680?token=eyJhbGciOiJIUzUxMiJ9.eyJpZCI6ImE2NGFiMzIyLTg0NzQtNDYyNi1iNmRmLTJvZGFkMTQ4OGFiMSIsImRhdGEiOi99LCJyZW5kb20iOiJmMThmYzYyYjYWE3NzIzZmJjY2RiN2RiNGMzNWZkYWRmZSJ9>

[.2GquoVhSxA7VuvDxTrl_rZ7MJBSLcS3kOsgRcsV-T3wyFIApDO_6_jUS8e9fTL5IvyN2zrOEAE49avdeugyEvg](https://doi.org/10.5281/zenodo.10949376)

References

1. The MaCh3 Collaboration, mach3-software/mach3: v1.0.0-beta (2024). <https://doi.org/10.5281/zenodo.10949376>
2. M.A. Acero et al. (NOvA), Phys. Rev. D **110**, 012005 (2024). [arXiv:2311.07835](https://arxiv.org/abs/2311.07835)
3. A. Gelman, Stat. Sci. **24**, 176 (2009)

4. B. Pontecorvo, Z. Eksp. Teor. Fiz. **53**, 1717 (1967)
5. Z. Maki, M. Nakagawa, S. Sakata, Prog. Theor. Phys. **28**, 870 (1962)
6. K. Abe et al. (T2K) (2025). [arXiv:2506.05889](https://arxiv.org/abs/2506.05889)
7. M. Tanabashi et al., Particle data group. Phys. Rev. D **98**, 030001 (2018)
8. F.J. Gilman, K. Kleinknecht, B. Renk, SSCL-597-REV2, CMU-HEP95-19 (1994)
9. Q.R. Ahmad et al., Sno collaboration. Phys. Rev. Lett. **87**, 071301 (2001)
10. Y. Fukuda et al., Phys. Lett. B **433**, 9–18 (1998)
11. O.M. O'Reilly, *Rotation Tensors* (Cambridge University Press, Cambridge, 2008), pp.163–205
12. H. Yokomakura, K. Kimura, A. Takamura, Phys. Lett. B **544**, 286 (2002). ([hep-ph/0207174](https://arxiv.org/abs/hep-ph/0207174))
13. S.P. Mikheyev, A.Y. Smirnov, Sov. J. Nucl. Phys. **42**, 913 (1985)
14. L. Wolfenstein, Phys. Rev. D **17**, 2369 (1978)
15. J. Pan, J. Sun, X.G. He, Int. J. Mod. Phys. A **34**, 1950235 (2020). [arXiv:1910.06688](https://arxiv.org/abs/1910.06688)
16. M. Freund, Phys. Rev. D **64**, 053003 (2001)
17. P.B. Denton, J. Gehrlein, J. High Energy Phys. **2023**, 090 (2023)
18. A.L. Moreno, [arXiv:2401.12829](https://arxiv.org/abs/2401.12829) (2024)
19. R.L. Workman, Others (Particle Data Group), PTEP **2022**, 083C01 (2022)
20. C. Jarlskog, Phys. Rev. Lett. **55**, 1039 (1985)
21. J.F. Fortin, N. Giasson, L. Marleau, Phys. Rev. D **94**, 115004 (2016). [arXiv:1609.08581](https://arxiv.org/abs/1609.08581)
22. J.F. Fortin, N. Giasson, L. Marleau, JHEP **04**, 131 (2017). [arXiv:1702.07273](https://arxiv.org/abs/1702.07273)
23. A. de Gouvea, H. Murayama, Phys. Lett. B **747**, 479 (2015). [arXiv:1204.1249](https://arxiv.org/abs/1204.1249)
24. M. Tanimoto, A.I.P. Conf. Proc. **1666**, 120002 (2015)
25. W. Grimus, L. Lavoura, J. High Energy Phys. **2008**, 106–106 (2008)
26. Y. Shimizu, M. Tanimoto, K. Yamamoto, Mod. Phys. Lett. A **30**, 1550002 (2015)
27. P.B. Denton, R. Pestes, J. High Energy Phys. **2021**, 139 (2021)
28. S. Abe et al., Phys. Rev. Lett. **100**, 221803 (2008)
29. K. Abe et al. (T2K), Nature **580**, 339 (2020). [Erratum: Nature 583, E16 (2020)], [arXiv:1910.03887](https://arxiv.org/abs/1910.03887)
30. G. Cowan, K. Cranmer, E. Gross, O. Vitells, Eur. Phys. J. C **71**, 1554 (2011). [Erratum: Eur.Phys.J.C 73, 2501 (2013)], [arXiv:1007.1727](https://arxiv.org/abs/1007.1727)
31. K. Abe et al. (T2K) (2025). [arXiv:2506.05889](https://arxiv.org/abs/2506.05889)